Geophys. J. R. astr. Soc. (1975) **42,** 489–517

Tidal Computations for Morecambe Bay

R. A. Flather and N. S. Heaps

(Received 1974 October 7)

Summary

A numerical finite-difference technique for computing tides in areas of shoaling water has been established and used to calculate the M_2 tide in Morecambe Bay. An essential feature of the method is the representation of drying banks, which appear as the water level falls on the ebb, and which are re-submerged on the flood as the level rises again. Since the non-linear advective acceleration should be important in shallow water, schemes for incorporating these terms are examined and the influence of advection on the tide assessed.

In a series of tests, the open sea tides applied to the outer boundary of the numerical bay model were taken first from existing tidal charts, then from calculations with a larger-scale encompassing model, and finally from observations of current. In each case, the computed tidal elevations within the Bay turned out to be in satisfactory agreement with those obtained from observations. However, it is significant that, in the first case, inaccuracy of the input tidal distribution deduced from charts gives rise to erroneous currents near the boundary.

1. Introduction

The use of numerical finite difference models to determine water movements in inshore coastal areas presents several problems not normally encountered in modelling larger, deeper sea regions. These problems stem, in the main, from the relative shallowness of bays and estuaries. If the nearshore area is fairly flat then the rise and fall of sea level associated with tides or storm surges can produce large excursions of the shore line, while isolated sandbanks may also be exposed and re-submerged. Thus the pattern of motion may change radically with elevation, flow being confined to deep channels when the level is low and setting across the intervening banks when these are covered. Further, the shallow water gives rise to important effects due to non-linear terms in the governing hydrodynamical equations. Thus, Charnock & Crease (1957) presented a dimensional analysis showing advection to be important in the equations of motion when the elevation of the water surface above the undisturbed level is comparable with the mean depth. The importance of the variation with time of water depth and frictional dissipation should also be mentioned: here, the validity of the standard quadratic law of bottom stress is questionable since the associated term contains a singularity when the water depth vanishes.

If the shoaling regions are not in themselves of interest, the above problems may be avoided by attempting to parameterize the absorption of energy which occurs

there (Proudman 1941; Hendershott & Speranza 1971; Bennett 1974). Otherwise, the difficulties remain to be overcome.

A number of difference schemes for shallow water computations have been proposed. Reid & Bodine (1968) introduced a method for calculating tides and storm surges using simplified equations in which advection and the rotation of the Earth were omitted. Here, the coastal boundary, constrained to follow mesh lines, was made to advance or retreat across the calculation grid in discrete steps with the rise or fall of water level. A zero flow condition was applied on the coastal boundary. Further, in order to permit the initial flooding of a dry grid element and to represent the flow over submerged barriers, empirical formulae based on the flow over weirs were adopted. The method was applied successfully to the computation of two hurricane surges in Galveston Bay, Texas.

Sielecki & Wurtele (1970) described a scheme for integrating the non-linear shallow-water equations over a sloping bottom of arbitrary configuration, using any of at least three finite-difference formulations. No lateral boundary conditions of zero normal flow are required in the sense referred to above, the shore line being determined by the computation at each time step. Thus, in this approach, the dynamical equations are solved so that the fluid determines its own level above the bottom of the basin at every point of space and time. The location of coastal boundaries through time is one outcome of this procedure, accounting for the presence of drying banks in shallow tidal areas.

Forming part of their comprehensive water quality simulation model for Jamaica Bay, New York, Leendertse & Gritton (1971) used a method of computation for tides in shoaling water employing an alternating-direction implicit difference technique for solving the full hydrodynamical equations. As in the approach of Reid & Bodine (1968), the boundary moves in discrete steps following the grid lines. By using drying conditions more restrictive than simply zero local water depth, Leendertse & Gritton found that they could suppress much of the computational noise generated by the discrete boundary movements. However, the procedure is complicated, partly because of the implicit form of their difference scheme which makes it necessary to recompute the motion in one or more complete rows of the grid when an element becomes dry.

Recently, Ramming (1972) has presented results from a model of the Elbe estuary incorporating drying banks, though no details of the numerical technique are given.

In the present paper, a new finite difference method for tidal computations in shallow water is described in full. As in the procedures of Reid & Bodine and Leendertse & Gritton, the land–sea boundary follows mesh lines and moves in discrete steps across the grid. A new set of conditions, not only testing the local water depth but also examining the slope of the free surface, is employed to regulate the process by which a wet point (one at which the water depth is positive) becomes dry and the opposite process by which a dry point (one at which the water depth is zero) becomes wet. In this, unreal discrete movements of the boundary with short period, causing a point to alternate between being wet and dry, are prevented. This procedure is incorporated into a simple explicit finite difference representation of the equations omitting advection (Scheme 1, described in Section 2). The form of the quadratic law of bottom stress is modified in order to impose an upper limit on frictional dissipation as the water depth diminishes. Two extensions of the method, using ' angled derivatives ' proposed by Roberts & Weiss (1966) to take account of advection, are given (Schemes 2 and 3, described in Section 3).

Morecambe Bay, containing large areas of sandbanks exposed at low tide, provides a suitable test area for the proposed techniques. The latter have been used to compute the M_2 tide in the region. Results obtained are discussed and compared with observations (Section 4). In particular, a comparison between the numerical solutions with and without advection is made. Further, the perennial problem of

determining open boundary conditions for sea models is examined in relation to the model of Morecambe Bay, and in this respect the advantages and disadvantages of using elevations from published cotidal charts, elevations derived from larger encompassing models, or direct observations of current, are discussed.

2. Basic equations and the finite difference scheme with drying

The equations of continuity and depth mean motion for co-oscillating tides on a flat rotating sea are

$$\frac{\partial \zeta}{\partial t} + \frac{\partial}{\partial x}(Hu) + \frac{\partial}{\partial y}(Hv) = 0, \tag{1}$$

$$\frac{\partial u}{\partial t} + u\frac{\partial u}{\partial x} + v\frac{\partial u}{\partial y} - fv + \frac{ku(u^2+v^2)^{\frac{1}{2}}}{H} + g\frac{\partial \zeta}{\partial x} = 0, \tag{2}$$

$$\frac{\partial v}{\partial t} + u\frac{\partial v}{\partial x} + v\frac{\partial v}{\partial y} + fu + \frac{kv(u^2+v^2)^{\frac{1}{2}}}{H} + g\frac{\partial \zeta}{\partial y} = 0, \tag{3}$$

where the notation is:

x, y Cartesian co-ordinates in the horizontal plane of the undisturbed sea surface,

t time,

ζ elevation of the sea surface,

u, v components of the depth mean current in the directions of increasing x, y respectively,

H total depth of water $= h+\zeta$,

h undisturbed depth of water,

f Coriolis parameter, assumed constant,

k coefficient of bottom friction,

g acceleration of the Earth's gravity.

The depth mean currents are defined as

$$u = \frac{1}{H}\int_{-h}^{\zeta} u'\,dz, \qquad v = \frac{1}{H}\int_{-h}^{\zeta} v'\,dz$$

where u', v' are components of horizontal current at depth z below the sea surface. In order to obtain the depth-averaged form of the advective terms in (2) and (3) it has to be assumed that the currents do not vary significantly in the vertical so that

$$\int_{-h}^{\zeta} u'^2\,dz = Hu^2, \qquad \int_{-h}^{\zeta} u'v'\,dz = Huv, \qquad \int_{-h}^{\zeta} v'^2\,dz = Hv^2.$$

The high rate of frictional dissipation in shallow seas causes disturbances to be damped quite rapidly so that after a short time the influence of initial conditions becomes negligible in comparison with effects introduced on the seaward boundary during the ensuing motion. Taking advantage of this, co-oscillating tides may be

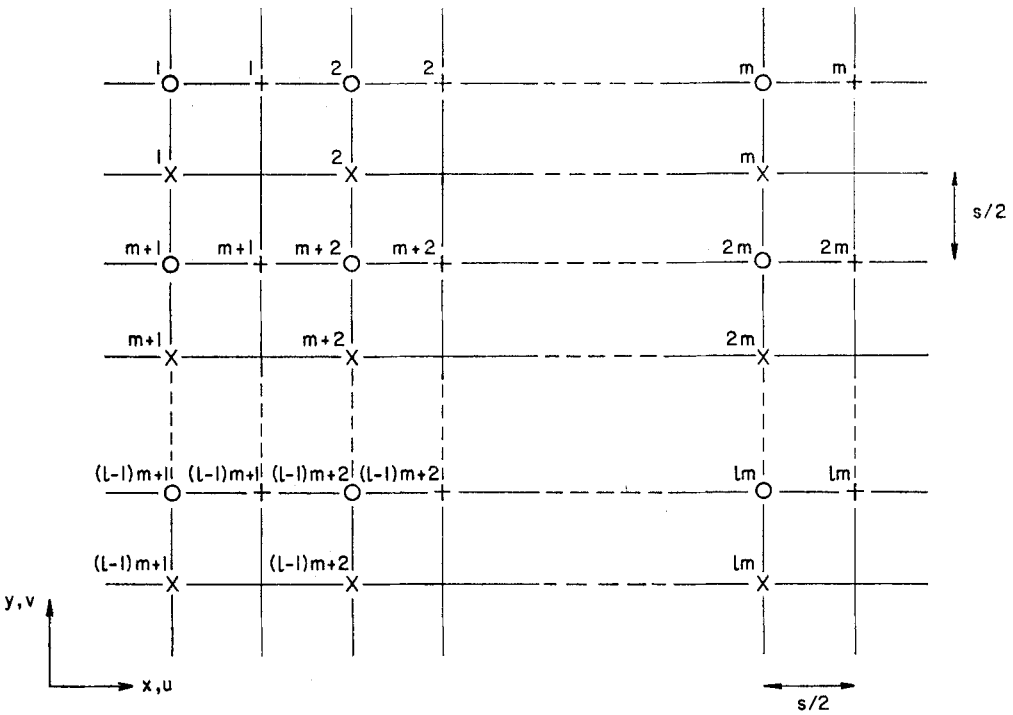

FIG. 1. The finite difference grid used in the numerical solution of the hydrodynamic equations showing the numbering system for the mesh points; ○, ζ-point; +, u-point; ×, v-point.

generated from an initial state of rest

$$\zeta = u = v = 0 \quad \text{at} \quad t = 0 \tag{4}$$

allowing a sufficient time for the tidal regime to become established. The tide is introduced along the open sea boundary by specifying either elevation as a function of position and time

$$\zeta = \hat{\zeta}(x, y, t) \tag{5}$$

or the normal component of current

$$q_n = \hat{q}_n(x, y, t) \tag{6}$$

where $q_n = u\cos\alpha + v\sin\alpha$ and α denotes the inclination of the outward directed normal to the axis of x. The coastal boundary condition is taken to be

$$q_n = 0 \quad \text{at} \quad H(x, y, t) = 0 \tag{7}$$

so that the location of the boundary is determined by the water level and depth distribution and the boundary moves with the rising and falling tide.

The problem is then to solve equations (1)–(3) to find the tidal variations of ζ, u, v over the sea given the changing distribution of elevation or current along the seaward boundary. A finite difference scheme for the numerical solution of this problem is now described.

A system of grid lines and the corresponding network of grid points is introduced to facilitate the numerical solution. The lines are drawn distance $s/2$ apart parallel to the co-ordinate axes (Fig. 1). Points are of three types: those denoted by a circle at each of which ζ is evaluated (ζ-points), those marked by a + sign at each of which u

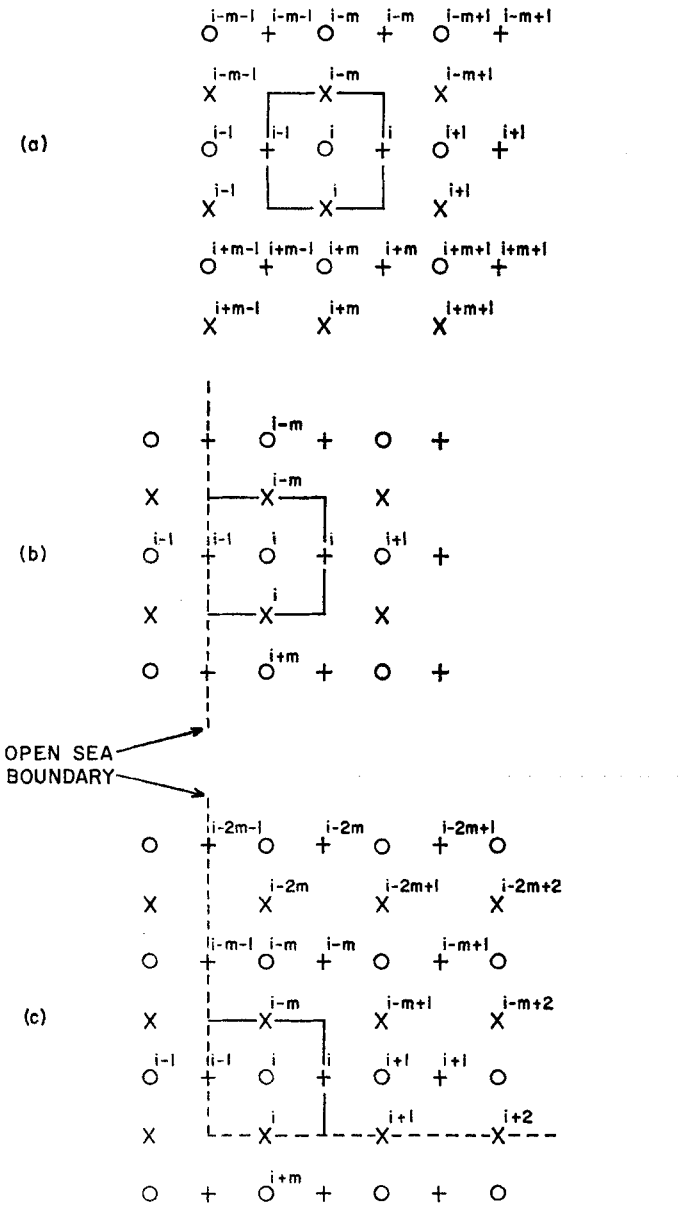

FIG. 2. Basic mesh elements consisting of squares of side s situated (a) within the area covered by the model, (b) adjacent to a y-directed open sea boundary, and (c) at a convex corner formed by the junction of segments of x-directed and y-directed open boundary, the area covered by the model lying in the first quadrant. Every mesh element has a u-point on each of its y-directed sides, a v-point on each of its x-directed sides and a ζ-point at its centre.

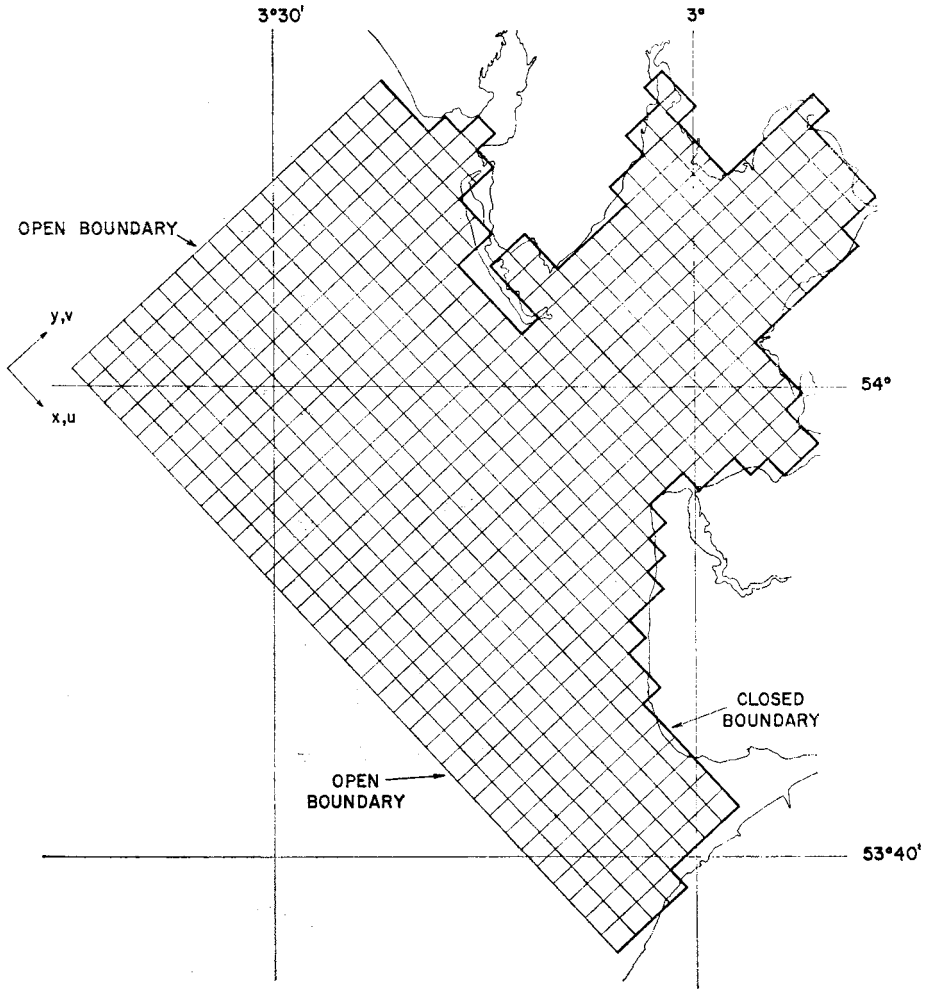

FIG. 3. Finite difference grid for the calculation of tides in Morecambe Bay allowing for drying banks. Input tides are prescribed along open boundaries of the model and the associated co-oscillation in the Bay determined.

is evaluated (u-points) and those marked by a $\times$ sign at each of which v is evaluated (v-points). The points of each type form a rectangular array of l rows and m columns and are numbered

$$i = 1(1)m,\ m+1(1)2m,\ 2m+1(1)3m,\ \ldots,\ \overline{l-1}m+1(1)lm$$

—counting point by point from left to right along each row, moving downwards from one row to the next.

The grid system covers inclusively the sea region under consideration. A basic mesh element, representing a fundamental area of sea, may be regarded as consisting of a square of side s with a u-point on each of its y-directed sides, a v-point on each of its x-directed sides, and a ζ-point in the middle (Fig. 2(a)). Our assembly of such elements for Morecambe Bay is shown in Fig. 3. Land and open-sea boundaries are modelled by the sides of mesh elements.

Discrete values of the variables are identified by subscripts as follows

$$\left.\begin{aligned} &\zeta = \zeta_i,\ h = h_i,\ H = H_i = h_i+\zeta_i \quad \text{at} \quad \zeta\text{-point } i,\\ &u = u_i \quad \text{at} \quad u\text{-point } i,\\ &v = v_i \quad \text{at} \quad v\text{-point } i. \end{aligned}\right\} \tag{8}$$

The basic equations (1)–(3) may now be represented by finite-difference approximations. Here a simplified scheme (Scheme 1) is described, in which the advective terms in (2) and (3) are neglected. The treatment of advection is dealt with separately in Section 3. We write:

$$\{\zeta_i(t+\tau)-\zeta_i(t)\}/\tau = -\{d_i(t)u_i(t)-d_{i-1}(t)u_{i-1}(t)+e_{i-m}(t)v_{i-m}(t)-e_i(t)v_i(t)\}/s, \tag{9}$$

$$\{u_i(t+\tau)-u_i(t)\}/\tau = f\tilde{v}_i(t)-ku_i(t+\tau)\{u_i^2(t)+\tilde{v}_i^2(t)\}^{\frac{1}{2}}/D_i(t) - g\{\zeta_{i+1}(t+\tau)-\zeta_i(t+\tau)\}/s, \tag{10}$$

$$\{v_i(t+\tau)-v_i(t)\}/\tau = -f\tilde{u}_i(t+\tau)-kv_i(t+\tau)\{\tilde{u}_i^2(t)+v_i^2(t)\}^{\frac{1}{2}}/E_i(t) - g\{\zeta_i(t+\tau)-\zeta_{i+m}(t+\tau)\}/s, \tag{11}$$

where

$$d_i = \tfrac{1}{2}(H_i+H_{i+1}), \qquad e_i = \tfrac{1}{2}(H_i+H_{i+m}),$$

$$D_i = \max(d_i, H_0), \qquad E_i = \max(e_i, H_0),$$

$$\tilde{u}_i = \tfrac{1}{4}(u_{i-1}+u_i+u_{i+m-1}+u_{i+m}), \qquad \tilde{v}_i = \tfrac{1}{4}(v_{i-m}+v_{i-m+1}+v_i+v_{i+1}),$$

τ being a small time increment and H_0 a postulated minimum depth for the denominator in the frictional term which could otherwise contain a singularity at $H = 0$. Thus, as defined above, D_i is taken to be the maximum of d_i and H_0 and therefore never falls below the value H_0. Similarly for E_i. This modification terminates the growth of frictional dissipation before it becomes too large and before the depth of fluid becomes so small that boundary layer considerations on which the quadratic law is based are no longer applicable. When taken in the order indicated, (9), (10) and (11) may be solved explicitly to determine ζ_i, u_i, v_i at time $t+\tau$ from known values at the earlier time t, thereby advancing the solution by one time step. Repeated solution of the equations allows the motion to be built up through time in the usual way starting from initial conditions based on (4) which take the form

$$\zeta_i(0) = u_i(0) = v_i(0) = 0. \tag{12}$$

Account is taken of drying in the iterative procedure by carrying out tests before each u and v calculation to determine whether the associated grid point is either ' wet ' or ' dry '. If the point is dry then the current is set to zero as in (7). If the point is wet, a new value of u or v is calculated by solving the equation of motion. The procedure, in which ε is a postulated height, may be summarized as follows:

if (i) $H_i(t+\tau) > 0$ and $H_{i+1}(t+\tau) > 0$ so that $d_i(t+\tau) > 0$

or (ii) $H_i(t+\tau) > 0$ and $H_{i+1}(t+\tau) \leqslant 0$ and $d_i(t+\tau) > 0$ and $\zeta_i(t+\tau)-\zeta_{i+1}(t+\tau) > \varepsilon$

or (iii) $H_i(t+\tau) \leqslant 0$ and $H_{i+1}(t+\tau) > 0$ and $d_i(t+\tau) > 0$ and $\zeta_{i+1}(t+\tau)-\zeta_i(t+\tau) > \varepsilon$

then calculate $u_i(t+\tau)$ from (10),

otherwise set $u_i(t+\tau) = 0$;

if (i) $H_i(t+\tau) > 0$ and $H_{i+m}(t+\tau) > 0$ so that $e_i(t+\tau) > 0$

or (ii) $H_i(t+\tau) > 0$ and $H_{i+m}(t+\tau) \leqslant 0$ and $e_i(t+\tau) > 0$

and $\zeta_i(t+\tau) - \zeta_{i+m}(t+\tau) > \varepsilon$

or (iii) $H_i(t+\tau) \leqslant 0$ and $H_{i+m}(t+\tau) > 0$ and $e_i(t+\tau) > 0$

and $\zeta_{i+m}(t+\tau) - \zeta_i(t+\tau) > \varepsilon$

then calculate $v_i(t+\tau)$ from (11),

otherwise set $v_i(t+\tau) = 0$.

The above tests only allow flow to occur at a current point when certain conditions on both depth and elevation gradient are satisfied there. Otherwise, with the current set to zero, conditions corresponding to a drying situation obtain.

Provision is also made for permanent land boundaries to be specified. Applying condition (7) in finite difference form we take $u_i = 0$ for all time at each u-point i on a y-directed boundary, and $v_i = 0$ for all time at each v-point i on an x-directed boundary.

Provision must be made for the application of open boundary conditions by specifying tidal elevation as in (5) or current as in (6). Consider first the case of elevation input. Elevation is prescribed for each ζ-point adjacent to and inside the model boundary. Then the equation of continuity for a grid element on a straight section of the boundary can be re-arranged to give the component of current across the boundary in terms of known quantities. For example, on a y-directed open boundary as in Fig. 2(b), (9) is written in the form

$$u_{i-1}(t) = \{d_i(t)u_i(t) + e_{i-m}(t)v_{i-m}(t) - e_i(t)v_i(t) + (s/\tau)\{\zeta_i(t+\tau) - \zeta_i(t)\}\}/d_{i-1}(t). \quad (13)$$

Then, assuming

$$d_{i-1} = \tfrac{1}{2}(h_{i-1} + \zeta_i + h_i + \zeta_i),$$

which in deep water involves only a small error since $h \gg \zeta$, all quantities on the right-hand side of (13) are known or prescribed and $u_{i-1}(t)$, the normal component of current at the boundary, can be found. At a convex corner of an open boundary, as in Fig. 2(c), two currents across the boundary, $u_{i-1}(t)$ and $v_i(t)$, are to be determined. The flux across the open boundary into the corner element is Qs, where

$$\begin{aligned} Q(t) &= d_{i-1}(t)u_{i-1}(t) + e_i(t)v_i(t) \\ &= d_i(t)u_i(t) + e_{i-m}(t)v_{i-m}(t) + (s/\tau)\{\zeta_i(t+\tau) - \zeta_i(t)\}, \end{aligned} \quad (14)$$

from continuity. The right-hand side of this equation contains known quantities only. To close the problem, one further constraint is needed. This is provided by using extrapolation based on Taylor series expansions from interior known values to give initial estimates $u_{i-1}^{(0)}$, $v_i^{(0)}$ for the required currents. In fact

$$u_{i-1}^{(0)} = -4u_{i-m} + 2(u_i + u_{i-m+1} + u_{i-2m} + u_{i-m-1}) - (u_{i+1} + u_{i-2m+1} + u_{i-2m-1}) + O(s^4), \quad (15)$$

$$v_i^{(0)} = -4v_{i-m+1} + 2(v_{i+1} + v_{i-m+2} + v_{i-2m+1} + v_{i-m}) - (v_{i+2} + v_{i-2m+2} + v_{i-2m}) + O(s^4). \quad (16)$$

Then, assuming

$$d_{i-1} = \tfrac{1}{2}(h_{i-1} + \zeta_i + h_i + \zeta_i) \quad \text{and} \quad e_i = \tfrac{1}{2}(h_i + \zeta_i + h_{i+m} + \zeta_i),$$

we take

$$\begin{aligned} v_i^{(1)} &= \{Q - d_{i-1}u_{i-1}^{(0)}\}/e_i, \\ v_i^{(2)} &= \tfrac{1}{2}\{v_i^{(0)} + v_i^{(1)}\}, \\ u_{i-1}^{(1)} &= \{Q - e_i v_i^{(2)}\}/d_{i-1}, \\ u_{i-1} &= \tfrac{1}{2}\{u_{i-1}^{(0)} + u_{i-1}^{(1)}\}, \\ v_i &= \{Q - d_{i-1}u_{i-1}\}/e_i, \end{aligned}$$

so that the final estimates $u_{i-1} = u_{i-1}(t)$ and $v_i = v_i(t)$ satisfy the equation of continuity (14). The computation of currents across the open boundary by the above methods is incorporated at appropriate stages in the iteration procedure.

When tidal current rather than elevation is the input variable, the values of $u_{i-1}(t)$, $v_i(t)$ discussed above are provided externally and, assuming the associated depths to be

$$d_{i-1} = \tfrac{1}{2}(h_{i-1}+h_i) \quad \text{and} \quad e_i = \tfrac{1}{2}(h_i+h_{i+m}),$$

all calculations within the model are based exclusively on equations (9)–(11).

3. Advective schemes

Consideration is now given to finite difference representations of the non-linear advective terms in equations (2) and (3). A number of stable explicit schemes for advection exist (Lax & Wendroff 1960; Crowley 1970; Sielecki & Wurtele 1970). The methods employed in the present paper are based on the 'angled derivative' approach of Roberts & Weiss (1966), which seeks to provide an approximation for the spatial derivatives of the advected quantity—in this case depth mean current—properly centred in space and time. The angled derivative is first illustrated by considering a simple example of advection in one dimension. Two extensions of the basic difference formulation, Scheme 1, employing angled derivatives to take account of the advective terms in the equations of motion are then described.

Take, as an example, the equation

$$\frac{\partial u}{\partial t} + u\frac{\partial u}{\partial x} = 0.$$

In the notation already defined, the finite difference representation of this equation, for the case in which the calculations proceed in the order of increasing i, might be taken as

$$\{u_i(t+\tau)-u_i(t)\}/\tau + \bar{u}_i(t)[\tfrac{1}{2}\{u_i(t+\tau)+u_{i+1}(t)\} - \tfrac{1}{2}\{u_{i-1}(t+\tau)+u_i(t)\}]/s = 0$$

where

$$\bar{u}_i = \tfrac{1}{4}(u_{i-1}+2u_i+u_{i+1}).$$

Here, use is made of the fact that when $u_i(t+\tau)$ is about to be calculated the values of $u_j(t)$ for $1 \leqslant j \leqslant m$ and $u_j(t+\tau)$ for $1 \leqslant j \leqslant i-1$ are known. The resulting difference approximation for $\partial u/\partial x$, the 'angled derivative', is correctly centred in time and space. In the next time step, Roberts & Weiss suggest that the direction of integration be reversed, so that calculations now proceed in the order of *decreasing* i, and the difference equation is

$$\{u_i(t+\tau)-u_i(t)\}/\tau + \bar{u}_i(t)[\tfrac{1}{2}\{u_i(t)+u_{i+1}(t+\tau)\} - \tfrac{1}{2}\{u_{i-1}(t)+u_i(t+\tau)\}]/s = 0$$

when the values of $u_j(t)$ for $1 \leqslant j \leqslant m$ and $u_j(t+\tau)$ for $i+1 \leqslant j \leqslant m$ are known. Both equations can be re-arranged to give $u_i(t+\tau)$ explicitly.

The above approach may be used in a number of ways to extend Scheme 1, described in Section 2, to take account of the advective accelerations. Perhaps the simplest method is to calculate changes in the components of depth-mean current over one time step due to advection alone and add them to the changes caused by other dynamical processes computed from equations (10) and (11), using the sums to update the current. This is our Scheme 2. The continuity equation (9) remains

unchanged but (10) and (11) are replaced by

$$\{u_i^*(t+\tau)-u_i(t)\}/\tau = f\tilde{v}_i(t)-ku_i^*(t+\tau)\{u_i^2(t)+\tilde{v}_i^2(t)\}^{\frac{1}{2}}/D_i(t) - g\{\zeta_{i+1}(t+\tau)-\zeta_i(t+\tau)\}/s \quad (17)$$

$$\{v_i^*(t+\tau)-v_i(t)\}/\tau = -f\tilde{u}_i^*(t+\tau)-kv_i^*(t+\tau)\{\tilde{u}_i^2(t)+v_i^2(t)\}^{\frac{1}{2}}/E_i(t) - g\{\zeta_i(t+\tau)-\zeta_{i+m}(t+\tau)\}/s \quad (18)$$

with the addition of, for odd time steps with i increasing,

$$\left.\begin{aligned}&\{u_i(t+\tau)-u_i^*(t+\tau)\}/\tau\\ &\quad = -\frac{1}{2s}\bar{u}_i^*(t+\tau)\{u_{i+1}^*(t+\tau)-u_i^*(t+\tau)+u_i(t+\tau)-u_{i-1}(t+\tau)\}\\ &\qquad -\frac{1}{4s}[\{v_{i-m}^*(t+\tau)+v_{i-m+1}^*(t+\tau)\}\{u_{i-m}(t+\tau)-u_i(t+\tau)\}\\ &\qquad +\{v_i^*(t+\tau)+v_{i+1}^*(t+\tau)\}\{u_i^*(t+\tau)-u_{i+m}^*(t+\tau)\}],\end{aligned}\right\} \quad (19)$$

$$\left.\begin{aligned}&\{v_i(t+\tau)-v_i^*(t+\tau)\}/\tau\\ &\quad = -\frac{1}{4s}[\{u_i^*(t+\tau)+u_{i+m}^*(t+\tau)\}\{v_{i+1}^*(t+\tau)-v_i^*(t+\tau)\}\\ &\qquad +\{u_{i-1}^*(t+\tau)+u_{i+m-1}^*(t+\tau)\}\{v_i(t+\tau)-v_{i-1}(t+\tau)\}]\\ &\qquad -\frac{1}{2s}\bar{v}_i^*(t+\tau)\{v_{i-m}(t+\tau)-v_i(t+\tau)+v_i^*(t+\tau)-v_{i+m}^*(t+\tau)\},\end{aligned}\right\} \quad (20)$$

where

$$\bar{u}_i = \tfrac{1}{4}(u_{i+1}+2u_i+u_{i-1}), \qquad \bar{v}_i = \tfrac{1}{4}(v_{i-m}+2v_i+v_{i+m}),$$

and similar equations for even time steps with i decreasing. Equations (17) and (18) determine the temporary values $u_i^*(t+\tau)$ and $v_i^*(t+\tau)$ and then equations (19) and (20) determine $u_i(t+\tau)$, $v_i(t+\tau)$.

Alternatively, taking account of advection directly in the equations of motion (Scheme 3), (10) and (11) are replaced by
for odd time steps with i increasing, calculating u first then v:

$$\left.\begin{aligned}&\{u_i(t+\tau)-u_i(t)\}/\tau\\ &\quad = -\frac{1}{2s}\bar{u}_i(t)\{u_{i+1}(t)-u_i(t)+u_i(t+\tau)-u_{i-1}(t+\tau)\}\\ &\qquad -\frac{1}{4s}[\{v_{i-m}(t)+v_{i-m+1}(t)\}\{u_{i-m}(t+\tau)-u_i(t+\tau)\}\\ &\qquad +\{v_i(t)+v_{i+1}(t)\}\{u_i(t)-u_{i+m}(t)\}]\\ &\qquad +f\tilde{v}_i(t)-ku_i(t+\tau)\{u_i^2(t)+\tilde{v}_i^2(t)\}^{\frac{1}{2}}/D_i(t)-g\{\zeta_{i+1}(t+\tau)-\zeta_i(t+\tau)\}/s,\end{aligned}\right\} \quad (21)$$

$$
\begin{aligned}
&\{v_i(t+\tau)-v_i(t)\}/\tau \\
&\quad = -\frac{1}{4s}[\{u_i(t)+u_{i+m}(t)\}\{v_{i+1}(t)-v_i(t)\} \\
&\qquad +\{u_{i-1}(t)+u_{i+m-1}(t)\}\{v_i(t+\tau)-v_{i-1}(t+\tau)\}] \\
&\qquad -\frac{1}{2s}\bar{v}_i(t)\{v_{i-m}(t+\tau)-v_i(t+\tau)+v_i(t)-v_{i+m}(t)\} \\
&\qquad -f\bar{u}_i(t+\tau)-kv_i(t+\tau)\{\tilde{u}_i^2(t)+v_i^2(t)\}^{\frac{1}{2}}/E_i(t) \\
&\qquad -g\{\zeta_i(t+\tau)-\zeta_{i+m}(t+\tau)\}/s,
\end{aligned}
\qquad (22)
$$

and similar equations for even time steps with i decreasing, calculating v first then u.

Both the above schemes may be readily incorporated into the complete procedure described in Section 2. The treatment of land–sea boundaries and drying is unaffected by the inclusion of advection. However, since not all the values of current needed to solve equations (19)–(22) at flow points adjacent to open-sea boundaries are defined, it is necessary to omit the advective terms within a distance s of these boundaries. When this was done in the Morecambe Bay calculations some instability was introduced in the form of grid scale oscillations which appeared to originate from the corner of the open boundary (Fig. 3). Leaving out the advective accelerations within $3s$ of the boundary, so that the treatment of advection and of open-sea boundaries are decoupled, removes the instability. Although this omission is less than ideal, it is perhaps more acceptable than restrictions imposed by some other schemes: for example, Leendertse (1967) excludes advective accelerations within a distance s of *land* boundaries, where the water is likely to be shallow and therefore, according to dimensional analysis non-linear terms important.

4. Application to Morecambe Bay

(a) *The numerical model*

An account is now given of the application of the schemes described in the preceding sections to the problem of co-oscillating tides in Morecambe Bay.

The finite difference grid used in the model of Morecambe Bay is shown in Fig. 3. The basic rectangular array comprises 1188 elements with $l = 33$, $m = 36$ including one element outside all boundaries to provide the necessary storage of variables. The mesh spacing is $s = 1$ nautical mile $= 1853$ m. The open boundary is located outside the Bay in the eastern part of the Irish Sea. A permanent land boundary (see Section 2) is specified as shown so that motion takes place entirely within the region of the grid plotted.

The average depth h_i of the sea bed below mean sea level associated with each element was determined from charts and the array of these values used to plot the depth contours shown in Fig. 4. Perhaps the most striking feature of the resulting distribution is the prominent trough, the Lune Deep, on the south-east side of the entrance to the Bay proper. The greatest model depth, 41 m, occurs here. Also evident are the large areas of shallow water, with $h < 5$ m say, in the inner Bay, which make it essential to treat drying banks within the model. Channels associated with three rivers entering the Bay can be identified. They are the Lune lying ENE of the Lune Deep, with the Kent to the north-east and the Leven to the north separated by Cartmel Wharf, an extensive shallow area. The numerous smaller channels and gullies which appear on detailed charts of the region are not resolvable by a mesh of the present dimensions.

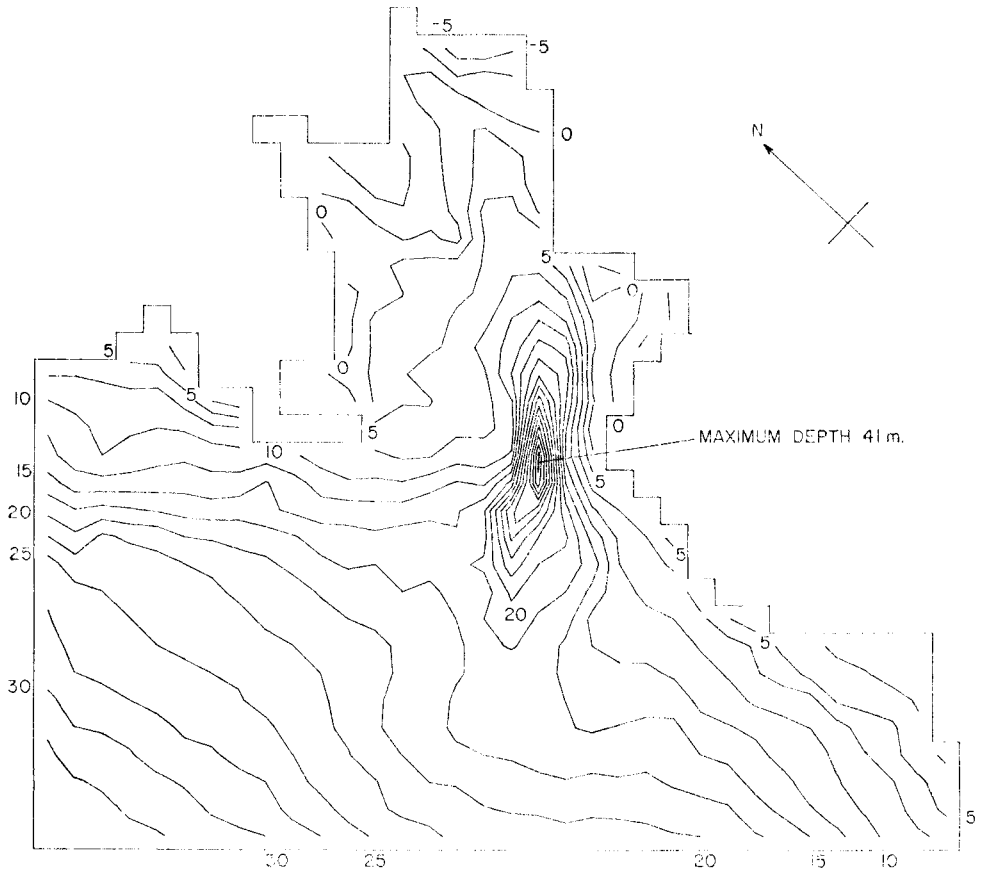

FIG. 4. Depth distribution in the model of Morecambe Bay with a contour interval of 2·5 m.

Taking the Courant–Friedrichs–Lewy criterion (Richtmyer & Morton 1967) in the form

$$\tau < s/\sqrt{(2gh)_{\max}} \tag{23}$$

as a guide to the maximum permissible time increment for stable difference solutions, and substituting $s = 1853$ m, $g = 9{\cdot}81$ m s^{-2}, $h_{\max} = 41$ m, yields $\tau < 65{\cdot}3$ s. The time step chosen was $\tau = 1/64$ lunar hour $= 58{\cdot}2$ s which satisfies (23) and in practice gave stable solutions with Schemes 1 and 2. In computations using Scheme 3 with the above value of τ grid scale oscillations of small amplitude were observed in the deepest part of the model. However, a reduction in time step to $\tau = 1/80$ lunar hour $= 46{\cdot}6$ s completely removed the slight instability and provided satisfactory results from this scheme. The time increment τ was taken in fractions of a lunar hour to make the period of the principal lunar semi-diurnal (M_2) constituent of the tides, investigated here, expressible as a convenient integer number of time steps.

Values of other parameters were taken as follows:

$$f = 1{\cdot}18 \times 10^{-4}\ \text{s}^{-1} \qquad k = 0{\cdot}0025$$

$$H_0 = 100\ \text{cm}, \qquad \varepsilon = 10\ \text{cm}.$$

Six runs were carried out using the various difference schemes presented in Sections 2 and 3 and with input data from a number of sources (see Table 1). In

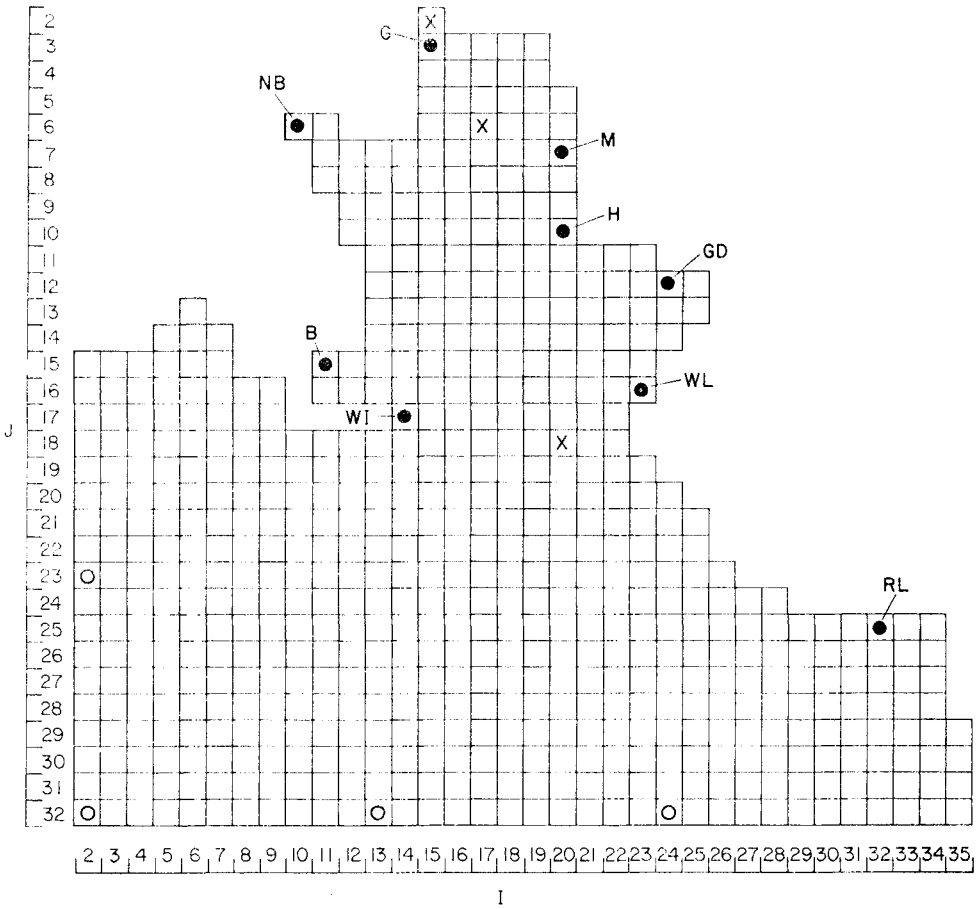

FIG. 5. The Morecambe Bay grid showing the location of points referred to in the text by their number (*I*, *J*); ●, point at which computed elevations are compared with observed elevations at a nearby port; ○, point at which computed currents are compared with observations of current; ×, point at which computed tidal profiles are plotted. Key to ports: G—Grange; NB—New Bridge; M—Morecambe; H—Heysham; GD—Glasson Docks; B—Barrow; WL—Wyre Light; WI—Walney Island; RL—Ribble Light.

runs A_1, A_2, A_3 elevation input was taken from a German tidal chart (Marine-observatorium Wilhelmshaven 1942); for run B elevations were read from the Admiralty tidal chart based on the work of Doodson & Corkan (1932) also quoted by Bowden (1955). The solution obtained by Mungall (1973) from a numerical model of the Irish Sea provided input for run C. Observations of current taken by the Institute of Coastal Oceanography and Tides during 1972 were used to estimate current input for run D.

The basic procedure followed in each case was to run the model starting either from an initial state of rest or from an initial state determined from an earlier solution. After computing through nine periods of the M_2 tide the difference between any elevation and the equivalent value at the same point one period earlier was generally found to be small—at most 0·1 cm—so that for practical purposes it could be assumed that the tidal regime had been established. Data from the tenth period was then taken as the required tidal solution, which could be analysed for harmonic components

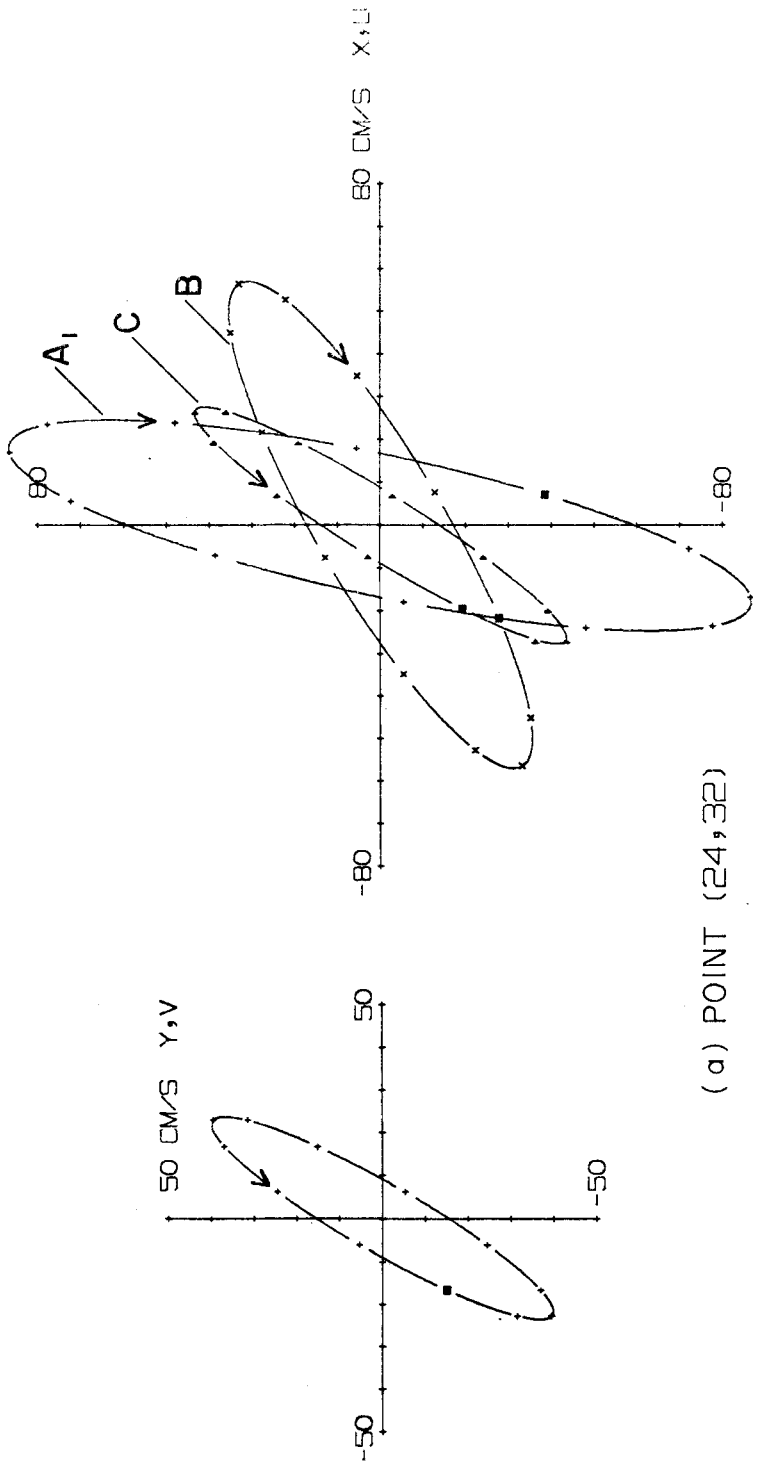

FIG. 6(a)

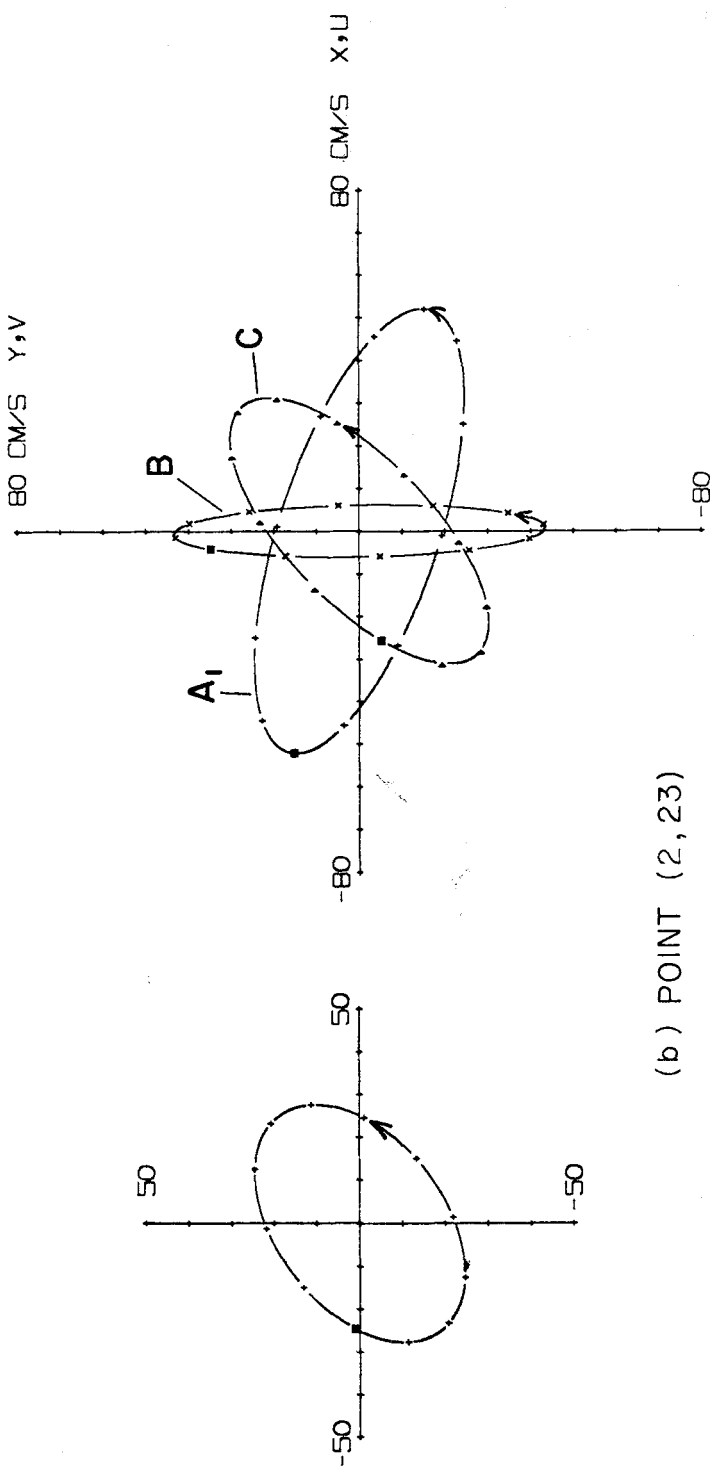

FIG. 6 Depth mean current ellipses for the M_2 tide derived from observations compared with computed ellipses from runs A_1, B and C. Two pairs of plots are shown corresponding to the two observation points (24, 32) and (2, 23). In each pair the observed ellipse is shown singly on the left and the three computed ellipses together on the right. On each ellipse a small square denotes the point corresponding to zero lunar hours and a symbol is drawn at intervals of one lunar hour. The arrow indicates the sense of rotation of the vector.

Table 1

Amplitude A (cm) and phase p° of the M_2 tide at Heysham calculated in various runs compared with constants from observational sources.

Observation

A	p	source
314·5	326·0	analysis by the Institute of Oceanographic Sciences of 1 year of observations
327·4	328·0	IHB tables

Calculation

A	p	run	scheme	input	source of input
334·1	323·5	A_1	1	ζ	tidal chart (Marineobservatorium Wilhelmshaven 1942)
333·3	323·5	A_2	2	ζ	tidal chart (Marineobservatorium Wilhelmshaven 1942)
333·3	323·5	A_3	3	ζ	tidal chart (Marineobservatorium Wilhelmshaven 1942)
327·2	328·5	B	1	ζ	tidal chart (Doodson & Corkan 1932)
339·4	328·2	C	1	ζ	Irish Sea model (Mungall 1973)
305·2	333·2	D	1	$\hat{q}_n$	observations

and assessed. Because the input to the model consists of a single harmonic constituent, M_2, the non-linearities in the governing equations of the system introduce only integer multiples of the fundamental frequency corresponding to a zero frequency component and the 'shallow water' constituents M_4, M_6, M_8 etc., so that at points not subject to drying straightforward Fourier analysis can be used to recover the M_2 tide from the total disturbance. At points which dry out and thus provide true water level data for only part of the tidal cycle some alternative method of analysis (see later) is required. Although analysis gives zero frequency and shallow water components, these cannot reasonably be expected to correspond to observations since they represent only the contributions generated within the Bay, no account being taken of these constituents entering the model across its open boundary.

(b) *Discussion of results*

The results obtained from tidal computations using the Morecambe Bay model are now discussed and compared with observations. Locations of points referred to in the discussion are shown in Fig. 5.

The amplitude and phase of the M_2 tide obtained by Fourier analysis from the solutions at point (20, 10) corresponding to Heysham, the site of the only permanent tide gauge within Morecambe Bay, are listed in Table 1. Note first that results from runs A_2 and A_3, using respectively Schemes 2 and 3 to take account of advection, are in agreement. This is generally true, though differences of the order of 0·1 cm in amplitude and 0·1° in phase occur at some places. These differences, due partly to the methods of incorporating advection and partly to the shorter timestep required by Scheme 3 which should result in a more accurate solution, are probably not significant.

Comparing the results from A_2 or A_3 with those from run A_1 gives an indication of the magnitude of the influence of advection. From Table 1, the amplitude of the M_2 tide at Heysham changes by only 0·8 cm when advection is omitted and the phase remains unaltered. In fact, nowhere does the amplitude change by more than 2·5 cm or the phase by more than 0·5°. The influence of advection on the fundamental constituent, then, is surprisingly small in view of the supposed importance of the terms in shallow water. However, since the advective terms are non-linear it might be argued that, through interaction, they would produce greater changes in the harmonics M_4, M_6 and so on, which changes would be evident in the total calculated

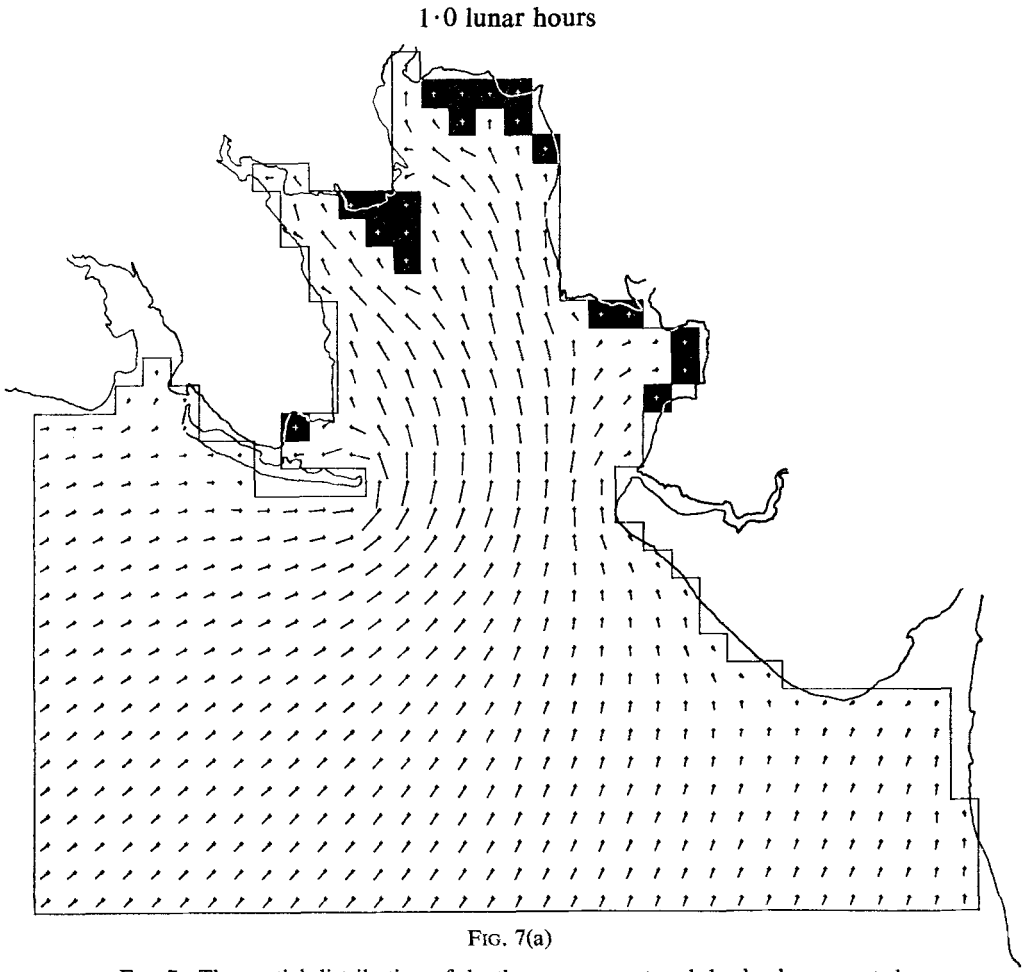

FIG. 7(a)

FIG. 7. The spatial distribution of depth mean current and dry banks computed in run D shown at intervals of two lunar hours ((a) to (f)) over a tidal cycle. The shaded areas are dry. A vector of length s (the distance between the origins of adjacent vectors) corresponds to a current of 100 cm s^{-1}.

elevations. An examination of the results produced some justification for this view, the greatest elevation difference due to advection being 6·6 cm. This is still small, however, amounting to perhaps 2 per cent of the tidal amplitude in the Bay.

The effect of advection on currents is generally more noticeable, the greatest influence being confined to an area off the southern tip of Walney Island. Here changes of 20 cm s^{-1} in magnitude and 10° in direction result from the inclusion of advection. It is significant that in this area the curvature of the currents is considerable and their magnitude greater than 100 cm s^{-1}, circumstances in which Brettschneider (1967) suggested that advection would be important.

The constants for Heysham, listed in Table 1, from runs A_1, B and C using Scheme 1 show discrepancies arising from the differences in tidal input elevation which are substantially greater than those due to the omission of advection. Although each source of elevation input gave apparently sensible results in the interior of the Bay on the basis of the comparison of constants with those obtained from observations (Table 1), the pattern of currents outside Morecambe Bay itself depended strongly on he input used. Observations of current taken at four stations along the model open boundary (see Fig. 5) provided the possibility of checking the solutions. The

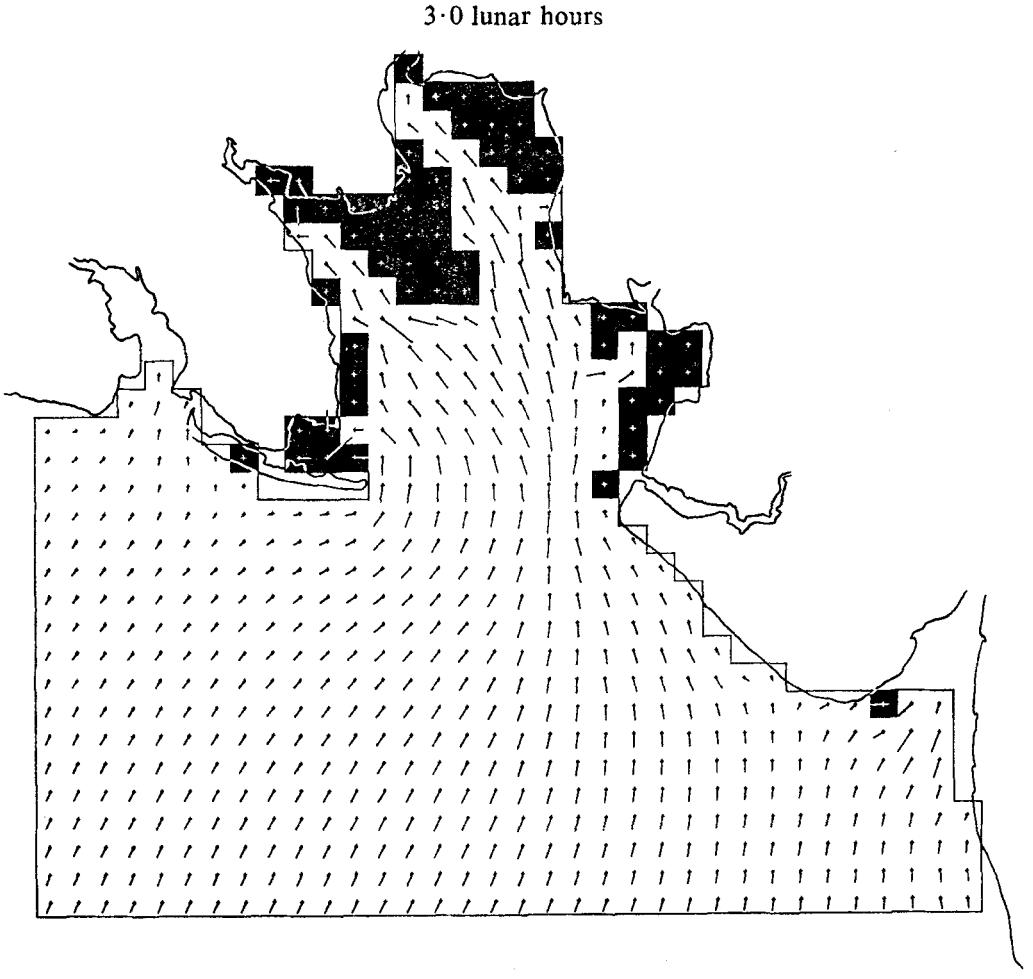

FIG. 7(b)

observational data, comprising 20 days of hourly values of east-going and north-going components of current from eight current meters (three on the rig at point (2, 32); two each at points (13, 32) and (2, 23); one meter at point (24, 32)) had first to be analysed into tidal constituents. For the M_2 constituents thus obtained, vertical profiles of the horizontal current components consisting of straight line segments were drawn by assuming that the current measured by the top meter was representative of the layer between this meter and the free surface and that the vertical gradient of current between the lowest two meters continued to the sea bottom. Estimates of the components of depth mean current were then made. For the station at point (24, 32), at which the water depth allowed only one current meter to be deployed, the depth mean current was assumed equal to the measured current. The resulting components of depth mean current were used to plot tidal ellipses which were compared with equivalent ellipses computed in runs A_1, B and C. Fig. 6 shows two examples of this comparison. It is clear that serious discrepancies exist between some of the computed results and the observations. Consistently the best agreement with observations is obtained from run C, which employed elevation input taken from the Irish Sea tidal model of Mungall (1973). However, neither the results of run A_1 using the German chart nor run B using the Admiralty chart can be considered

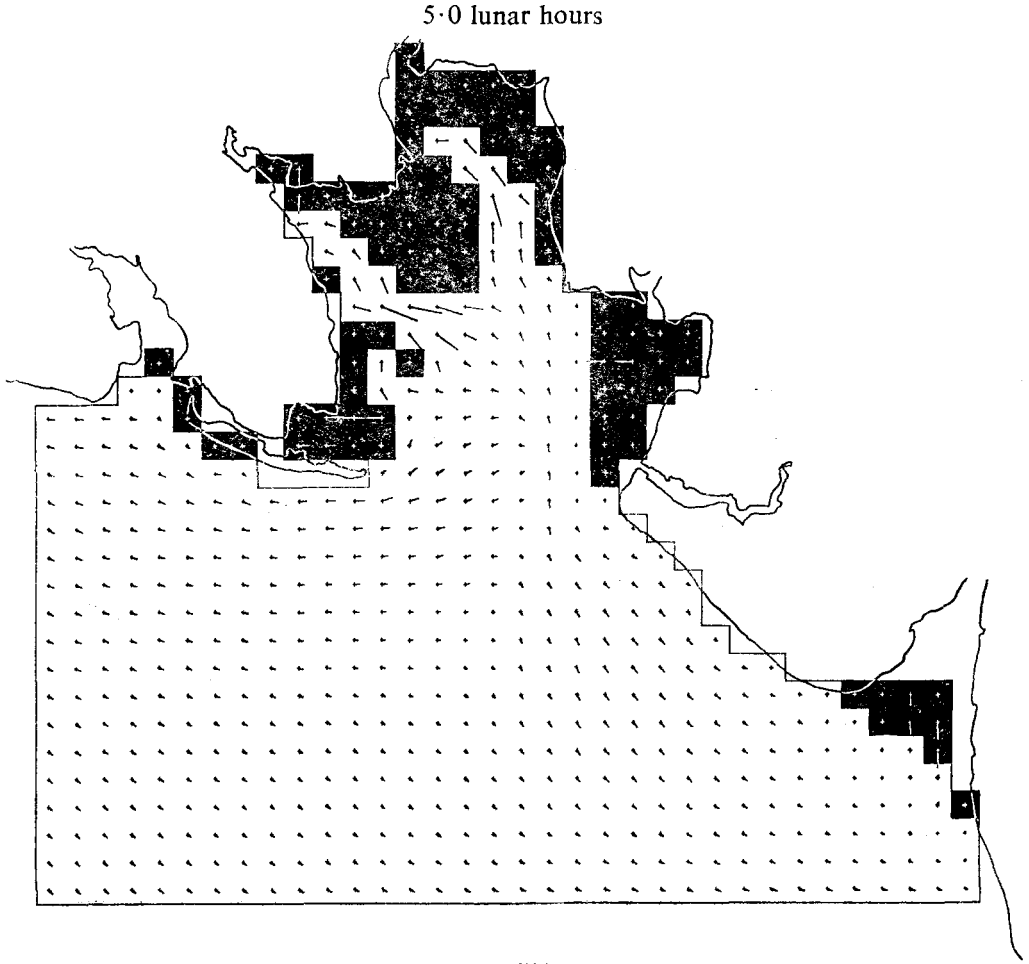

FIG. 7(c)

satisfactory. The discrepancies in these cases, due to the incorrect distribution of the input tidal elevation, can be attributed in part to the actual inaccuracy of the charts and also to the lack of detail they provide making difficult the preparation of the necessary numerical data. It would appear that slightly wrong curvatures of the co-tidal lines can cause significant discrepancies in the field of tidal currents. The success of run C in reproducing the observed tidal ellipses points to the usefulness of larger less detailed encompassing models in providing input data needed for hydrodynamical model investigations of coastal regions.

Further use was made of the current observations to provide input for run D in the form of the distribution along the open boundary of the normal component of current, $\hat{q}_n$ (see Section 2). The spatial distribution of the appropriate component of current was estimated by fitting a quadratic variation to the three data points (2, 32), (13, 32) and (24, 32) on the x-directed boundary, and a linear variation to the two data points (2, 32) and (2, 23) on the y-directed boundary. Because the ultimate mean water level inside the Bay depends on the initial elevations, and no compensating net transport of water in or out is permitted, an additional running-in procedure was needed in this case. Thus, a complete run was carried out and the results analysed only to find that the mean water level was as much as 20 or 30 cm above or below the assumed mean sea level. The initial conditions for the run were then corrected by

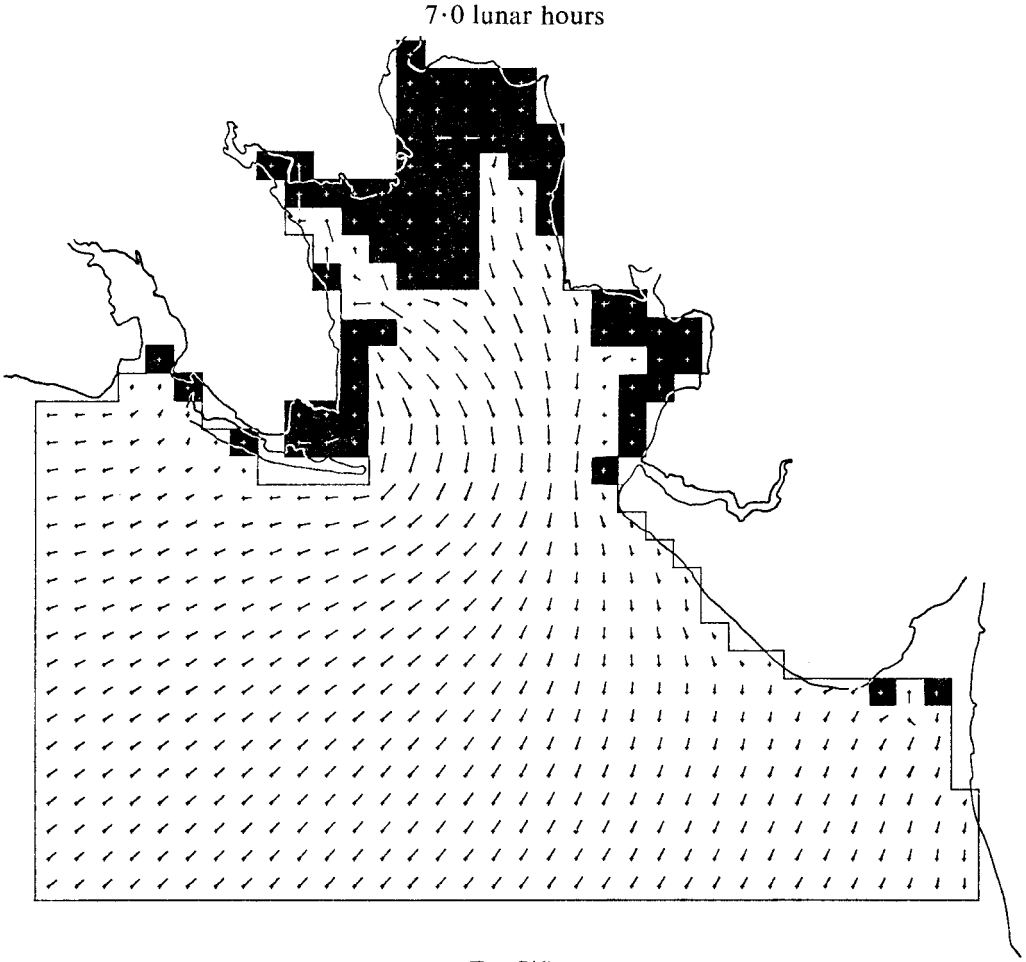

FIG. 7(d)

subtracting or adding the average height difference to the elevations at all 'wet' grid points and the run repeated. The mean water level was then sufficiently close, within 1 or 2 cm say, of the model datum. The solution from run D is now used to illustrate further aspects of the motion.

The spatial distributions of depth mean current and dry banks deduced from run D are shown at intervals covering one tidal period in Fig. 7. The time of each plot is given in lunar hours after transit of the Moon across the Greenwich meridian. Here dry grid elements within the model are shaded and for each elevation point, indicated by a small cross, a vector with the cross at its origin is drawn representing the current obtained by averaging values at adjacent flow points. From the description of the drying procedure in Section 2, the currents in dry elements should be zero, though in one or two instances in Fig. 7 it may be noted that elements for which a non-zero vector has been drawn have been designated as dry. The vectors referred to represent movements of very small amounts of water left behind as the tide recedes and since these pools are in no way connected to the main body of the Bay, it was decided for simplicity to show the associated grid boxes as dry areas. The successive exposure of greater areas of dry banks as the ebb proceeds (hours 1–5) and the subsequent re-covering of these areas with the flood (hours 7–11) is readily seen in this sequence of diagrams. The computed motion is in qualitative agreement with

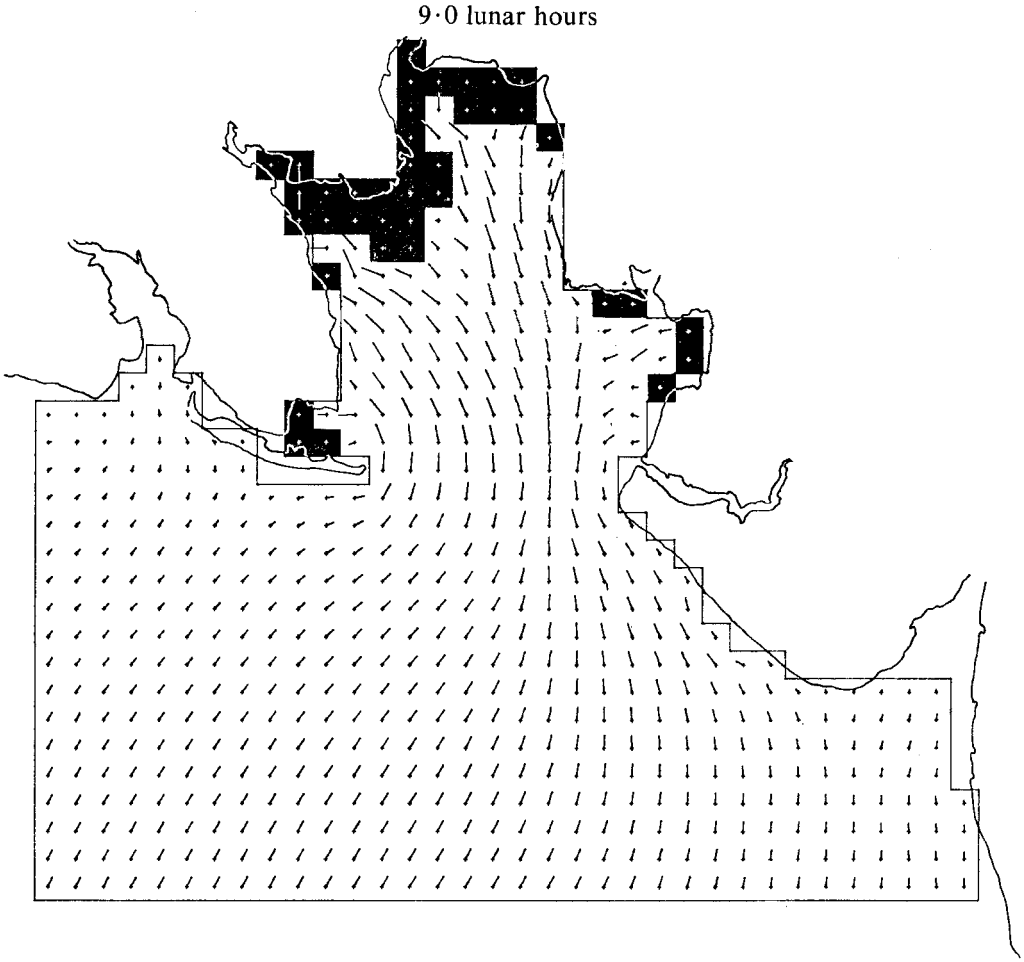

FIG. 7(e)

observed conditions in Morecambe Bay as described by Phillips (1968, 1969), the Hydraulics Research Station (1970), and the West Coast of England Pilot (1960). Outside the Bay the computed current vectors rotate anticlockwise. Within the Bay motion is confined to the main river channels near to low water but sets across the intervening banks when these are covered. The flood appears first on the NW side of the entrance around the southern tip of Walney Island at 5 lunar hours when on the SE side the last of the ebb still persists. Similarly the ebb begins near Walney Island at about 11 lunar hours when the tide is still flooding along the Lancashire coast and through the Lune Deep. The ebb in the river channels continues for some time after the tide has turned in the main body of the Bay, a consequence of the distortion of the tidal wave in shallow water. The distortion is illustrated in Fig. 8, which contains sets of tidal profiles computed at three points located along the channel from the Lune Deep to the River Kent (see Fig. 5). In Fig. 8, the sea surface elevation, ζ, magnitude of the tidal current, R, and direction of the current, θ, measured clockwise from North, are plotted against time in lunar hours. Variations at point (20, 18) in the Lune Deep are typical of deep water sites, the elevation profile being almost sinusoidal and the ebb and flood currents practically the same in magnitude and duration. An increased degree of asymmetry can be seen at point

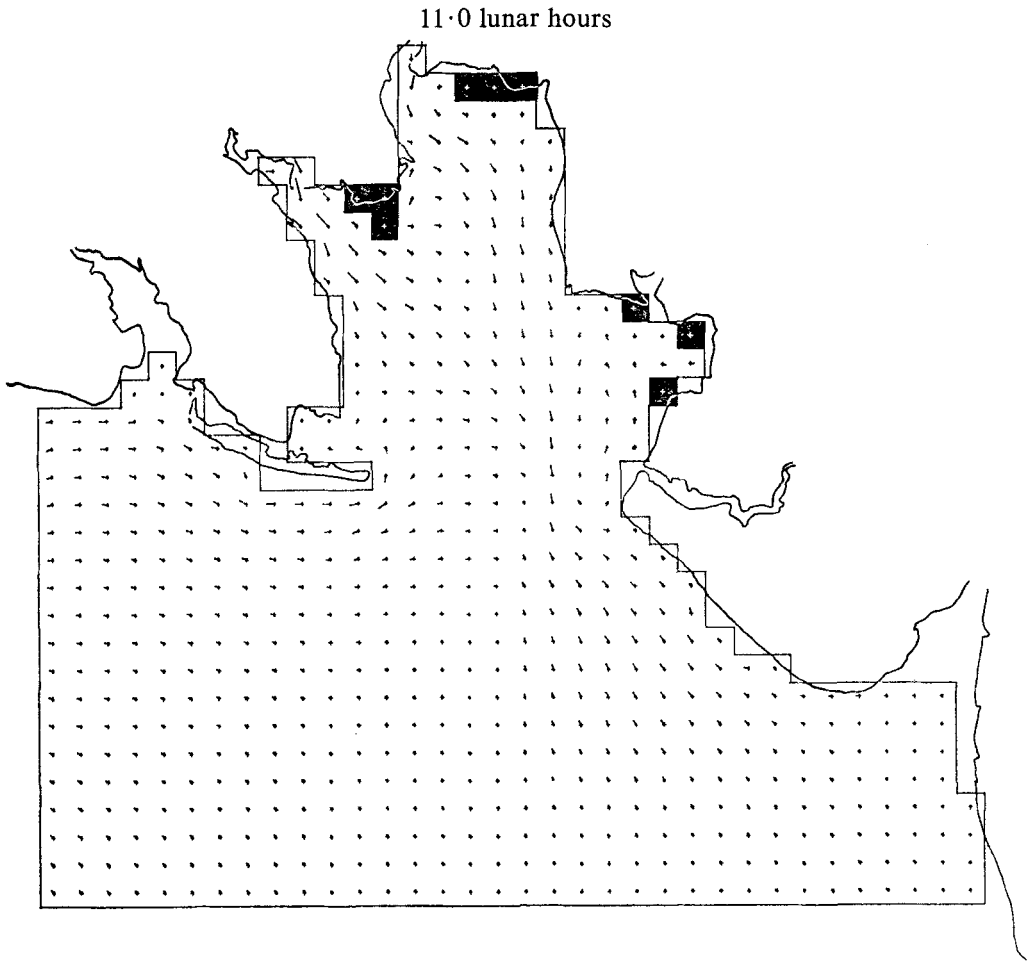

FIG. 7(f)

(17, 6) which comes close to drying at low water. The remaining point (15, 2) is dry for about 8½ lunar hours of the tidal period, ζ remaining constant and R being zero during this time. The distortion at (15, 2) is such that the flood lasts for only 1 lunar hour and the ebb for 2½ lunar hours.

The analysis of data from drying points such as (15, 2) to extract the M_2 tidal constants presents considerable difficulties. As mentioned earlier, straightforward Fourier analysis cannot be sensibly applied when less than one complete period of data is available. Harmonic analysis using a least squares technique similar to that used for actual tidal analysis proved successful when the span of data was reasonably long but gave less certain results for such points as (15, 2). Consequently it was decided that the time and height of high water (HW) rather than the amplitude and phase of M_2 should be used for comparisons between computations and observations. Table 2 contains the complete comparison for all existing data in Morecambe Bay. Observed or estimated HW is based directly on the M_2 constants from the sources stated; computed HW is found from total elevations including M_2 and its harmonics calculated in run D so that the comparison though useful is not precise. In view of the approximations involved the agreement can be considered satisfactory.

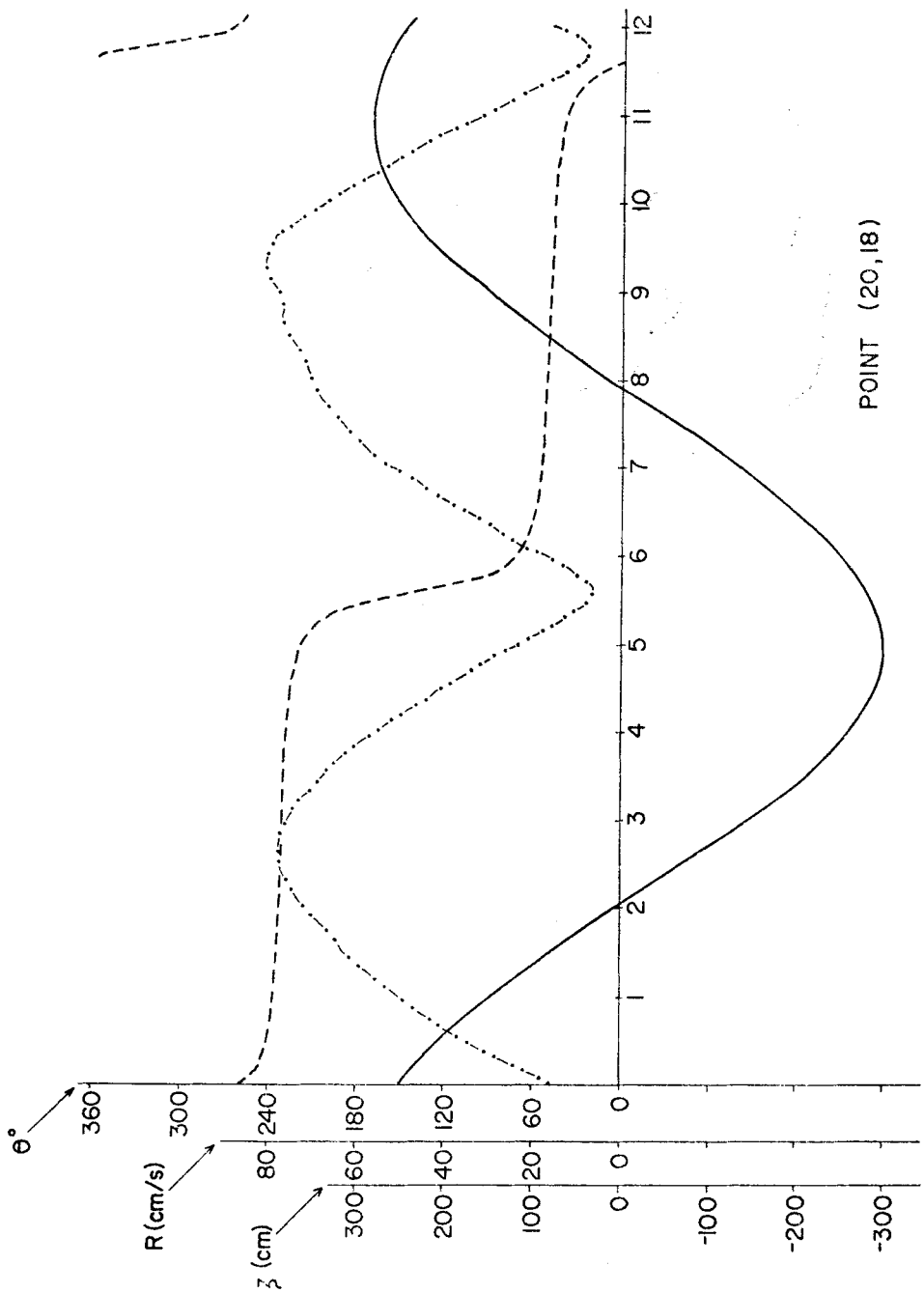

FIG. 8(a)

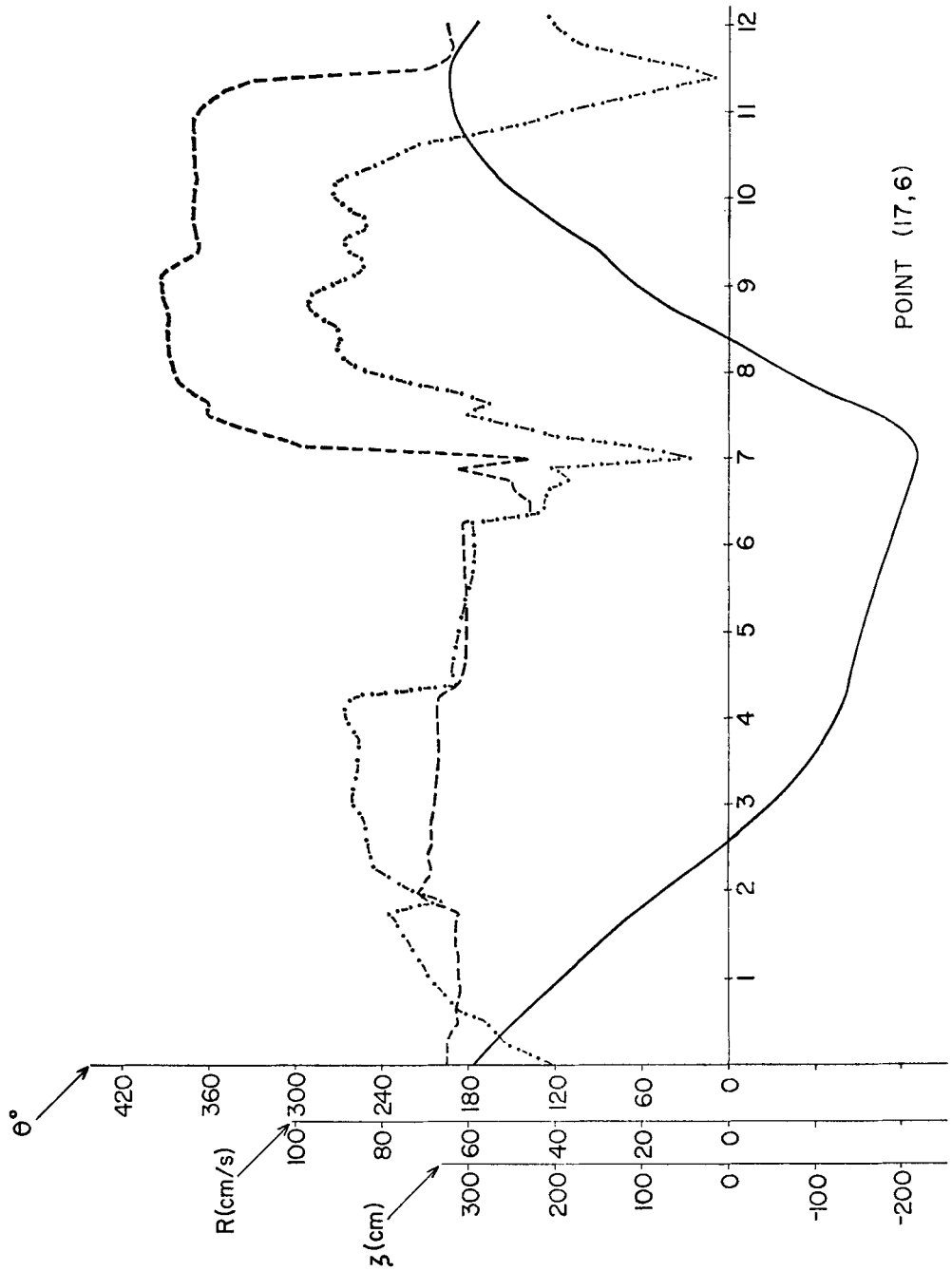

FIG. 8(b)

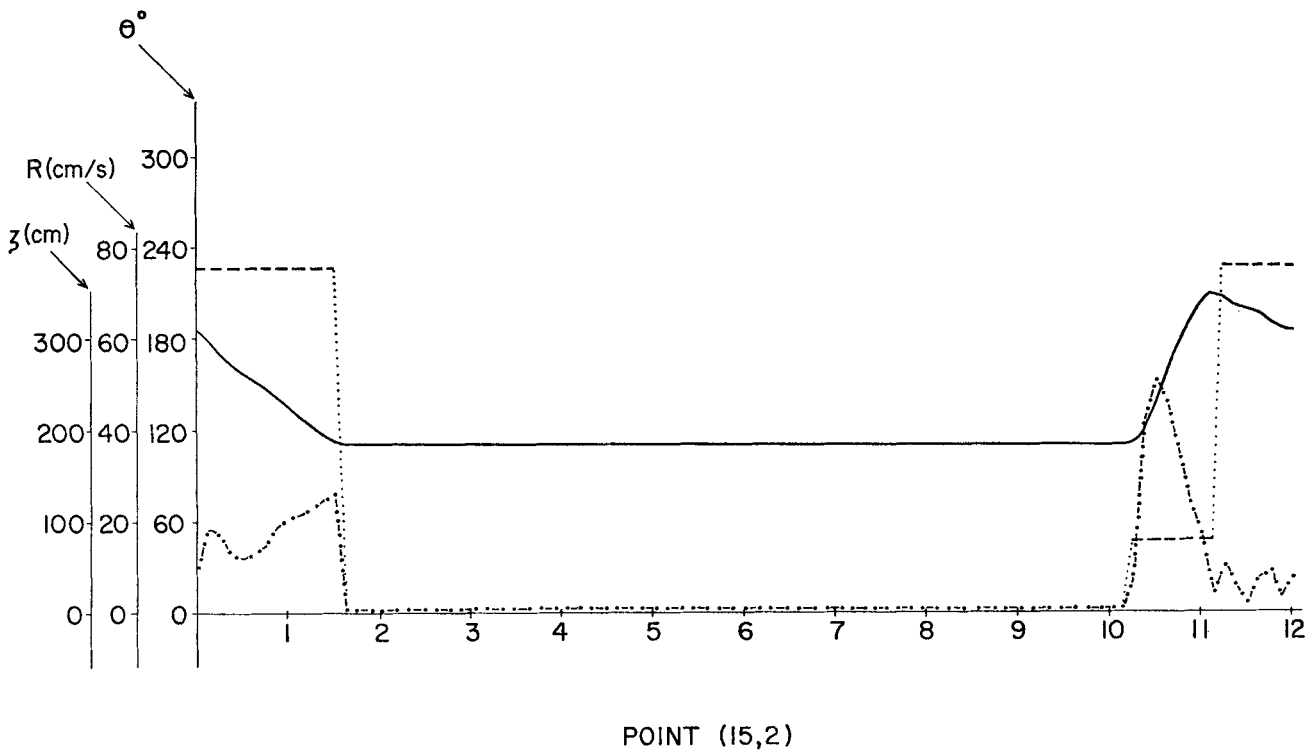

FIG. 8(c)

FIG. 8. Tidal profiles for 3 points between the Lune Deep and the River Kent computed in run D, illustrating the distortion of the tide as it propagates into shallow water. Elevation ζ (————), magnitude R of the depth mean current (·—··—··—··—·), and direction θ of the depth mean current measured clockwise from the north (– – – –) are plotted against time in lunar hours.

Table 2

*Comparison of height (cm) and time (lunar hours after lunar transit at Greenwich) of high water calculated in run D with values for the M_2 constituent only from other sources: *, estimated by Doodson & Corkan (1932); †, analysis by the Institute of Oceanographic Sciences of 1 year's observations; ‡, IHB tables.*

	Grid point (*I*, *J*)	Calculated Height	Calculated Time	Observed or estimated Height	Observed or estimated Time
Morecambe	(20, 7)	317·1	11·34	308	10·87*
Heysham	(20, 10)	305·8	11·31	314·5	10·87†
				327·4	10·93‡
Glasson Docks	(24, 12)	300·2	10·99	338	10·87*
Barrow	(11, 15)	304·5	11·00	304·3	10·99†
				310	10·80*
Wyre Light	(23, 16)	296·7	11·05	310	10·80*
Walney Island	(14, 17)	285·8	11·10	310	10·87*
Ribble Light	(32, 25)	281·4	11·05	300	10·47*

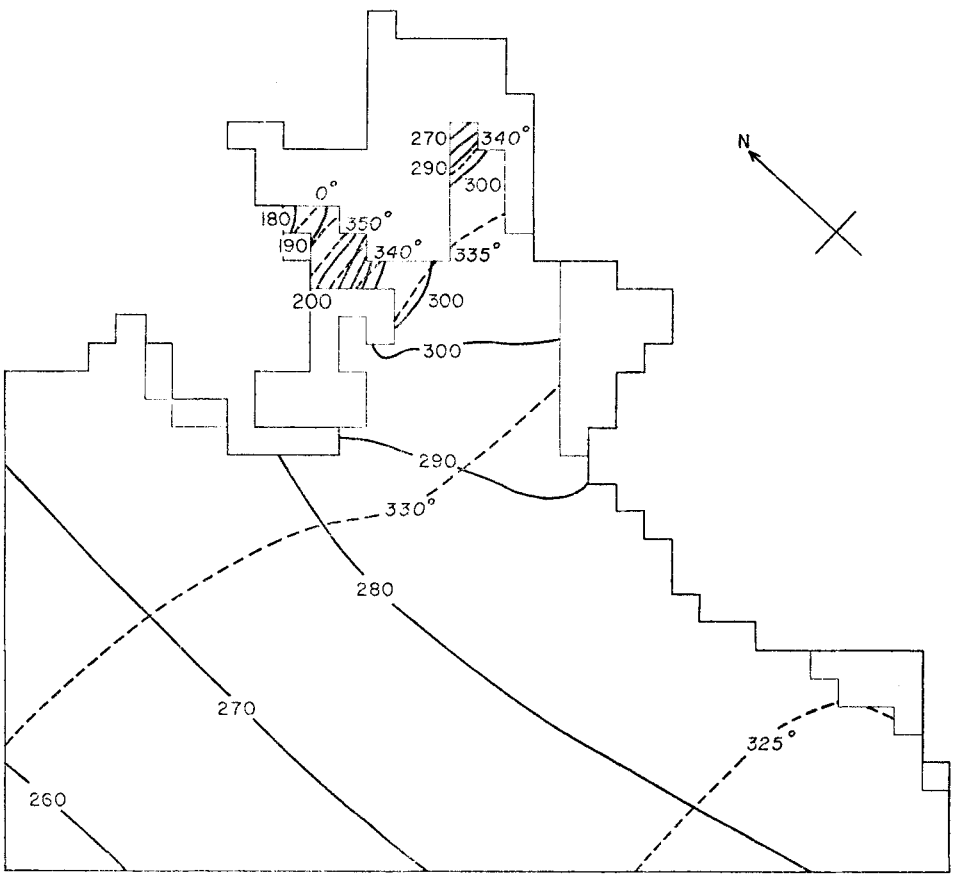

FIG. 9. Distribution of the M_2 tide in Morecambe Bay calculated in run D showing co-amplitude (————) and co-tidal (— — —) lines. The chart covers only those parts of the Bay not subject to drying. Amplitudes are given in centimetres.

To provide a check on the propagation of the tide within Morecambe Bay, a temporary tide gauge was installed by the Institute of Oceanographic Sciences at Grange-over-Sands near the mouth of the River Kent. One month of data was obtained and differences in the height and time of each HW between Grange and the permanent gauge at Heysham were found. The average value of each difference taken over a 29-day period then corresponds to the difference for a mean tide or for M_2 and could be compared with the equivalent difference computed using the model. The height and time differences from observations were respectively 43 cm and 11 mins; taking point (15, 3), see Fig. 5, as closest to the location of the Grange gauge, the computed height and time differences were respectively 39 cm and $9\frac{1}{2}$ mins. A similar check was made using data from a gauge at New Bridge at the outflow of the River Crake into the Leven. Height and time differences between HW at New Bridge and at Heysham were found, a mean value of each difference taken (this time over a period of 15 days), and the results compared with equivalent differences computed using the model. Unfortunately, the closest point to New Bridge (10, 6), see Fig. 5, is some two nautical miles downstream of the tide gauge so that the comparison is less satisfactory than that for Grange. The observed height and time differences were respectively 40 cm and 50 mins; the computed height and time differences were 20 cm and $52\frac{1}{2}$ mins. Despite the discrepancy in the height difference at New Bridge, the agreement is satisfactory and the close correspondence between observed and calculated time differences suggests that the model at least reproduces the tidal progression in to the inner Bay very well.

Finally, M_2 tidal constants obtained by Fourier analysis from the results of run D were used to construct a tidal chart covering all the parts of Morecambe Bay which do not dry. Fig. 9 shows this chart. It is interesting to note the increase in amplitude from the open boundary to the area around Heysham and the subsequent decrease, probably associated with the transfer of energy from M_2 to its harmonics, in the shallowing channels of the Kent and Leven.

5. Concluding remarks

A numerical finite difference technique for tidal computations in shallow and shoaling water has been introduced and used to calculate the M_2 tide in Morecambe Bay. The basis of the scheme is to determine afresh at each time step the position of the land–sea boundary, thereby allowing the boundary to move. The drying banks which are exposed as the water level falls on the ebb and re-submerged as the level rises again on the flood are thus taken into account. Two extensions of the basic difference formulation employing the 'angled derivative' approach of Roberts & Weiss (1966) to represent the non-linear advective terms in the equations of motion have been examined. Comparisons of calculated results for Morecambe Bay with existing data and with some new observations of current and elevation taken for use in the present study confirm that the model reproduces adequately the main features of the mean tidal regime.

Several points which arose in the investigation and which may bear on future studies of tides in coastal waters should be mentioned in summary.

1. The overall influence of advection on the tidal regime in Morecambe Bay as determined by comparing solutions with and without the associated terms in the equations was found to be quite small, the effect on elevations being at most 2 per cent of the tidal amplitude. The effect on currents was somewhat larger and could be important locally. If, therefore, residual currents or effects arising from non-linear interactions in shallow water are of interest, then advective accelerations should no doubt be retained. In the present instance, errors in the M_2 tide introduced by omitting advection were smaller than errors arising from other sources.

2. Although the solutions calculated using elevation input data extracted from published charts were in reasonable agreement with the M_2 tide observed at Heysham, large discrepancies were found between computed and observed currents near the seaward limit of the model. The errors, which arise because the distribution of input elevations was incorrect, are due to real inaccuracy in the charts and also to the lack of detail they provide, a deficiency which makes the preparation of the necessary numerical data very difficult.

3. Remarkably good agreement was achieved between observed currents near the open boundary and currents computed in run C using elevation input derived from the Irish Sea model of Mungall (1973). Since the computed tidal constants at Heysham in this case were as accurate as those obtained from other runs, it can be concluded that a large-scale encompassing model may offer a most useful source of input data for detailed model studies of coastal areas.

4. Although depth mean current is seldom used as the input variable in numerical sea model studies, the practicability of using data in this form for tidal computations has been demonstrated in run D. The difficulty in ensuring that the proper volume of water is contained within the model initially and hence that the eventual mean sea level is correct is readily overcome by applying an adjustment to the initial field of elevations based on results of a preliminary run.

Acknowledgments

The authors are indebted to Mr J. E. Jones for writing graph-plotting programs used in presenting the computer results, to Dr J. M. Vassie for performing harmonic analyses of the current meter data, and to Miss Y. Spruce for preparing the figures for publication.

Thanks are also due to members of the staff of the Institute of Oceanographic Sciences for their work in taking the offshore current measurements and for installing and maintaining the temporary tide gauge at Grange-over-Sands.

Institute of Oceanographic Sciences,
Bidston Observatory,
Birkenhead, Cheshire L43 7RA.

References

Bennett, A. F., 1974. Parametric representation of tidal shallows, *Geophys. J. R. astr. Soc.*, **38,** 389–396.

Bowden, K. F., 1955. Physical oceanography of the Irish Sea, *Fishery Invest., Lond., Ser.* 2, **18,** No. 8, 67 pp.

Brettschneider, G., 1967. Anwendung des hydrodynamischnumerischen Verfahrens zur Ermittlung der M_2—Mitschwingungsgezeit der Nordsee, *Mitt. Inst. Meeresk. Univ. Hamburg* Nr. 7.

Charnock, H. & Crease, J., 1957. North Sea surges, *Sci. Prog., Lond.* **45,** 494–511.

Crowley, W. P., 1970. A numerical model for viscous, free surface, barotropic wind driven ocean circulations, *J. comp. Phys.*, **5,** 139–168.

Doodson, A. T. & Corkan, R. H., 1932. The principal constituent of the tides in the English and Irish Channels, *Phil. Trans. R. Soc. A*, **231,** 29–53.

Hendershott, M. C. & Speranza, A., 1971. Co-oscillating tides in long narrow bays; the Taylor problem revisited, *Deep-Sea Res.*, **18,** 959–980.

Hydraulics Research Station, 1970. Feasibility study of water conservation in Morecambe Bay, *Report EX*502, 4 vols.

Lax, P. & Wendroff, B., 1960. Systems of conservation laws, *Comm. pure appl. Math.*, **9**, 217–237.

Leendertse, J. J., 1967. Aspects of a computational model for long-period water-wave propagation, *The Rand Corporation, Santa Monica*, Calif., RM-5294-PR.

Leendertse, J. J. & Gritton, E. C., 1971. A water quality simulation model for well mixed estuaries and coastal seas: Vol. 11, Computation procedures, *The Rand Corporation, New York*, R-708-NYC.

Marineobservatorium Wilhelmshafen, 1942. Karten der harmonischen Gezeitenkonstanten für das Gebiet der Nordsee, Ausgabe A, Oberkommando der Kriegsmarine, Nr. 2752.

Mungall, J. C. H., 1973. *Numerical tidal models with unequal grid spacing*, PhD Thesis, University of Alaska.

Phillips, A. W., 1968. A sea bed drifter investigation in Morecambe Bay, *The Dock and Harbour Authority*, **48**, No. 571, 9–13.

Phillips, A. W., 1969. Sea-bed water movements in Morecambe Bay, *The Dock and Harbour Authority*, **49**, No. 580, 379–382.

Proudman, J., 1941. The effect of coastal friction on the tides, *Mon. Not. R. astr. Soc. geophys. Suppl.*, **5**, 23–26.

Ramming, H. G., 1972. Reproduction of physical processes in coastal areas, *Proc. Thirteenth Conf. on Coastal Engineering*, Vancouver, ASCE.

Reid, R. O. & Bodine, B. R., 1968. Numerical model for storm surges in Galveston Bay, *Proc. Am. S. Civil Eng., J. Waterways Harbors Div.*, **94**, 33–57.

Richtmyer, T. D. & Morton, K. W., 1967. *Difference methods for initial-value problems* (2nd ed.). John Wiley and Sons, New York.

Roberts, K. V. & Weiss, N. O., 1966. Convective difference schemes, *Maths. Comput.*, **20**, 272–299.

Sielecki, A. & Wurtele, M. G., 1970. The numerical integration of the non-linear shallow-water equations with sloping boundaries, *J. comp. Phys.*, **6**, 219–236.

West Coast of England Pilot, 1960. *Sailing directions*, Hydrographic Dept., Admiralty.